ACS APPLIED MATERIALS & INTERFACES

RESEARCH ARTICLE

www.acsami.org

Investigation of the Emission Mechanism in Milled $SrAl_2O_4$:Eu, Dy Using Optical and Synchrotron X-ray Spectroscopy

Sanjeev Kumar Kandpal,[†] Ben Goundie,[‡] Joshua Wright,[‡] Rachel A. Pollock,[‡] Michael D. Mason,[†] and Robert W. Meulenberg*[,‡,§]

[†]Department of Chemical and Biological Engineering, University of Maine, Orono, Maine 04469, United States

[‡]Department of Physics and Astronomy, University of Maine, Orono, Maine 04469, United States

[§]Laboratory for Surface Science and Technology, University of Maine, Orono, Maine 04469, United States

ABSTRACT: There currently exists much debate as to the active state related to the "long afterglow" effect in europium doped oxide materials. Redox couples that consist of $Eu^{+/2+}$ and $Eu^{2+/3+}$ are discussed, but no common answer is currently accepted. Here, we present a comparison of the optical properties of a commercially available $SrAl_2O_4$:Eu, Dy phosphor, as a function of nanoparticle size reduction via dry mechanical milling. X-ray and optical spectroscopic data indicate a significant decrease in phosphorescence efficiency and an increase in laser stimulated emission efficiency as near surface Eu^{2+} ions are oxidized to Eu^{3+} as a consequence of increased exposure during the milling process. These results show evidence only for $Eu^{2+/3+}$ oxidation states, suggesting the mechanism related to long afterglow effect does not arise from Eu^{+} species. We also suggest that size reduction, as a rule, cannot be universally applied to improve optical properties of nanostructures.

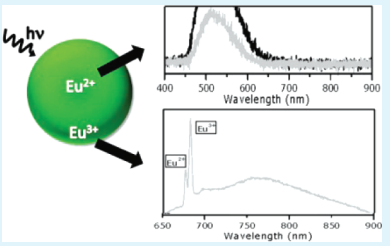

KEYWORDS: rare earth doping, EXAFS, electronic structure, thermoluminescence, long afterglow phosphorescence

INTRODUCTION

In recent years, rare earth doped particles have found widespread use as phosphors in commercial products ranging from temperature detection,[1] structural damage sensing,[2] emergency lighting, and even children's toys.[3] The attractiveness of these materials can generally be attributed to their bright long-lived visible phosphorescence, wavelength tunability, ease of synthesis, good chemical stability, and relative low cost. Increasingly, these materials are being investigated for applications requiring reduced particle dimensions, such as in thin films for optical or electronic devices,[4] or medical diagnostics.[5] Recent work suggests that some doped phosphors exhibit little degradation in optical efficiency at reduced dimensions; however, the emission mechanism in these systems is still controversial[6] and may be affected by particle size.[7] Typically, nanoscale phosphors are prepared by solid state reaction, vacuum deposition, or combustion methods,[8] which can be prohibitively expensive for most commercial applications. An alternative more cost-effective approach involves size reduction via mechanical milling. While this approach is not universally applicable to all nanomaterials, it may have value for nanoparticles where the property of interest is determined by the presence of dopant ions within the particle and not the final particle dimensions.

In this manuscript, we present a comparison of the optical properties of a commercially available $SrAl_2O_4$:Eu, Dy phosphor before and after milling. To improve dispersity, a low cost surfactant is also considered. Both X-ray and visible spectroscopic data is presented and used to describe the observed changes in optical efficiency. Our work suggests that size reduction leads to degradation of the phosphorescence and thermoluminescence of the phosphor but an increase in laser induced emission, providing further insight into the emission mechanism in this system.

EXPERIMENTAL METHODS

Sample Preparation. A 3 lb capacity benchtop ball mill was used to mechanically reduce the size of a commercially available $SrAl_2O4$:Eu, Dy phosphor (United Nuclear, LumiNova G-300). The mill was charged with ~0.31 cm diameter Alumina-silica beads (50% total capacity) and the dry granular phosphor (25% total capacity). Continuous milling was carried for 48 h where ~100 mg of test samples was extracted every 12 h. The samples were sized by transmission electron microscopy (TEM) and Dynamic Light Scattering (DLS, Zetasizer Nano) in water (data not shown). The milled samples exhibited a dramatic increase in solution stability with only minimal settling in 6 h. This procedure resulted in an apparent reduction in diameter from >1000 nm (volume weighted) to 150 nm after 12 h. For longer milling times, DLS data indicated a small increase in size, which, by analysis of TEM data, was attributed to aggregation of smaller particles. In a second trial, polyethylene glycol (MW 20 000) was added (5 wt % of phosphor) to improve particle dispersity during both the milling and sizing procedures. The resulting particles showed only a small additional decrease in size after 12 h,

Received: June 1, 2011
Accepted: August 4, 2011
Published: August 19, 2011

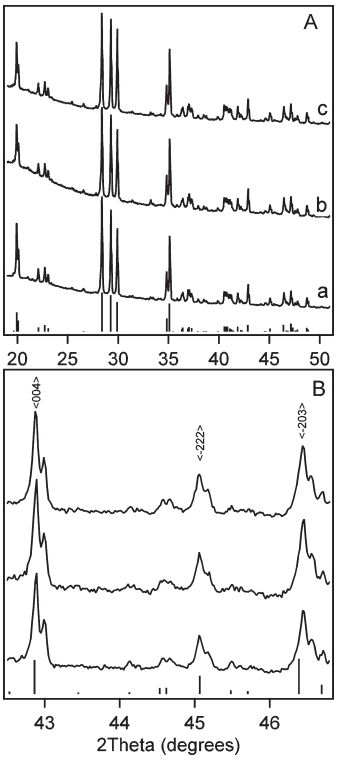

Figure 1. Powder X-ray diffraction measurements for the (a) original, (b) dry milled, and (c) PEG milled samples alongside the calculated peak intensities based on PDF card 04-010-5403 (bottom trace). The data in both panels are equivalent, with (B) plotting an expanded region to make peak shifts visible. Spectra are offset for clarity.

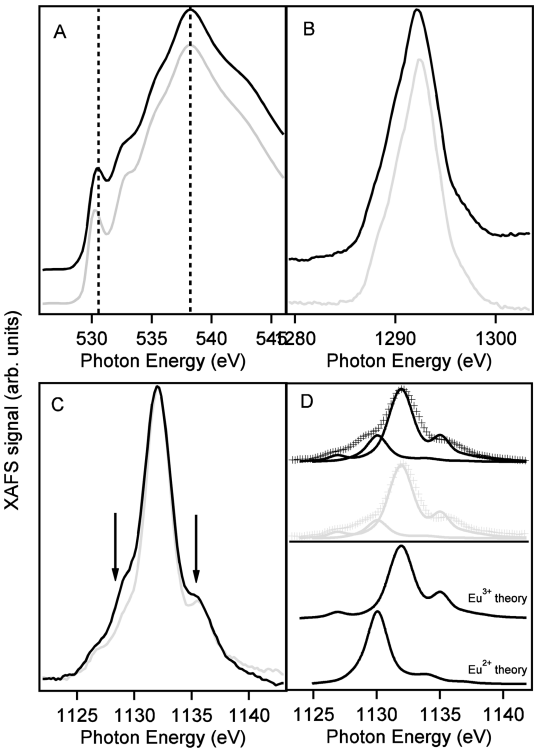

Figure 2. (A) O K-edge, (B) Dy M_5-edge, and (C)/(D) Eu M_5-edge XAFS of the as purchased (black) and 48 h dry milled (gray) samples. The bottom two traces in (D) are multiplet simulations of the Eu^{2+} and Eu^{3+}, respectively. Some spectra are offset for clarity.

reaching a limiting diameter of around 150 nm. Solution stability was further increased in these samples.

Characterization. *X-ray Diffraction.* Nanoparticle structure was studied using X-ray diffraction (XRD) by $\theta-2\theta$ scans with Cu Kα radiation using line focus on a PANalytical X′PertPro Diffractometer (Figure 1). In all the samples studied, the XRD peaks were well indexed to single phase monoclinic $SrAl_2O_4$ (PDF# 04-010-5403).

Synchrotron Methods. Soft X-ray absorption near edge spectroscopy (SXANES) was performed at beamline 8-2 at the Stanford Synchrotron Radiation Lightsource (SSRL), Stanford Linear Accelerator Center. Powders were affixed to carbon tape and inserted into an ultrahigh vacuum chamber. SXANES experimental measurements were taken at base pressures of less than 5×10^{-9} Torr. SXANES experiments were conducted using the total electron yield (TEY) detection method where the total photocurrent is measured as the photon energy is scanned through the absorption edges. The experimental energy resolution was ~0.10–0.20 eV for the various edges (O, K; Eu, $M_{4,5}$; Dy, $M_{4,5}$) studied in this letter. For the hard X-ray measurements, both X-ray absorption near edge spectroscopy and extended X-ray absorption fine structure were analyzed. X-ray absorption fine structure (XAFS) spectroscopy was performed at beamline 10-2 at the SSRL using Si(220) crystals detuned about 30%; a slit height of 2 mm was used. Powder samples were mounted on 5×10 mm pieces of Kapton tape. Eu L_3-edge XAFS spectra were collected at room temperature in partial fluorescence mode using a 13-element Ge detector to collect Eu Lβ fluorescence photons. I_0 was monitored using a nitrogen filled ionization chamber. An Eu foil was placed after the sample for energy calibration.

Optical Methods. For optical characterization, an equivalent mass (0.15 g) of the as purchased and 48 h milled samples was placed in a welled slide and capped with a standard coverslip. Samples were stored overnight, in the dark,[9] in a −80 °C freezer prior to characterization to ensure complete thermal deactivation consistent with previously reported methods.[10] Luminescence was generated under laser (473, 632 nm) or thermal excitation. A home-built confocal microscope equipped with a 0.85 NA air objective was used for optical excitation and signal collection. The resulting emission was directed to a 1/4 m spectrometer (Acton Instruments) and liquid nitrogen cooled CCD camera (Princeton Instruments, SPEC-10). Excitation power (6 mW) was held fixed for all samples at each wavelength, and spectra were similarly collected over constant integration periods. Phosphorescence spectra (10 s integration) were collected every 10 s for 1 h following a 10 s exposure to 473 nm radiation (6 mW). For photothermal emission, a software controlled hot plate was used to provide a well determined temperature ramp (~1 °C per second). Photothermal emission was collected via an optical fiber (Thorlabs, AFS105/125Y) placed in direct contact with the sample coverslip and directed to an avalanche photodiode module (EGG, SPCM). Total temperature dependent emission was determined by integrating each time sampled spectrum.

RESULTS AND DISCUSSION

As observed in Figure 1A, the structure of the doped $SrAl_2O_4$ is not strongly affected with milling; indeed, the monoclinic phase that occurs is the undoped material, present in all stages of

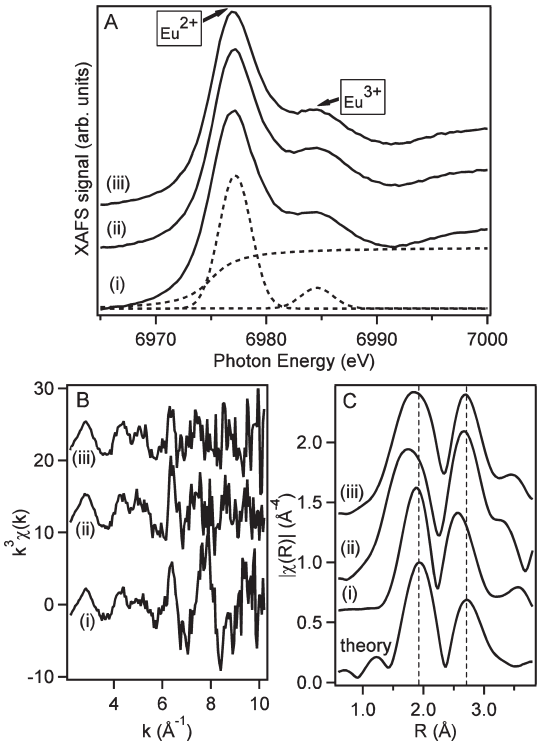

Figure 3. Eu L_3-edge (A) hard XANES, (B) k^3-weighted $\chi(k)$ EXAFS, and (C) Fourier transforms (not phase shift corrected) of the EXAFS for the (i) as prepared, (ii) dry milled, and (iii) PEG milled samples. The black dashed lines in (A) are described in the text. The bottom trace in (C) is the theoretical FT EXAFS of Eu:$SrAl_2O_4$. All spectra are offset for clarity.

the nanosized doped material. The large scale of Figure 1A, however, obscures any small changes that may occur in peak positions. Plotted in Figure 1B is an expanded region of the data in Figure 1A; notably, this expanded region encompasses peak indices of ⟨004⟩, ⟨222⟩, and ⟨−203⟩. The relationship between lattice plane spacing and lattice parameters for a monoclinic lattice is

$$\frac{1}{d^2} = \frac{1}{\sin^2\beta}\left(\frac{h^2}{a^2} + \frac{k^2\sin^2\beta}{b^2} + \frac{l^2}{c^2} - \frac{2hl\cos\beta}{ac}\right)$$

For the ⟨004⟩ peak, only the c parameter contributes to the lattice spacing while the other peaks have contributions from the other lattice parameters. Most notably, the ⟨−203⟩ peak exhibits a decrease in d-spacing with milling; this implies that the a lattice parameter changes as the particle size is reduced during the milling process. This suggests a reduction in bond length occurs in these materials (see EXAFS results, Figure 3).

Oxygen K-edge, Dy M_5-edge, and Eu M_5-edge SXANES are presented in Figure 2A,B,C/D, respectively. The O K-edge X-ray spectra for the as purchased and dry milled samples, in general, look similar, suggesting the local oxygen environment is not strongly affected with milling. The spectral features resemble those found in strontium oxide based materials[11] and do not agree with published O K-edge SXANES data for aluminum oxide,[12] europium oxide,[13] or lanthanum oxide.[14] Interestingly, however, we observe a shift in the pre-edge peak of ∼0.4 eV with milling. The pre-edge peak represents transitions from O 1s states to O 2p antibonding states hybridized with Eu 4f states.[15] A shift of ∼0.4 eV has been observed in the O K-edge XAS for $EuFeO_3$ when compared to $SmFeO_3$. This energy shift occurs because the electronic configuration of Sm is such that it contains one less f electron than Eu. Similar behavior is more than likely occurring in our materials. During milling, we observe an increase in Eu^{3+} species, especially on the surface (vida infra). As our spectroscopy is sensitive to the surface, a shift in ∼0.4 eV is consistent with "oxidation" of the Eu. The change in intensity may be simply due to a size effect due to changes in the multiple scattering processes.

The Dy and Eu M_5-edge data suggest that the codopant Dy exists in the 3+ oxidation state[4] while the Eu atoms exist in a mixed 2+/3+ oxidation state, agreeing with other reports on similar materials.[4,16] The fine structure in the Eu M_5-edge has been shown to provide a spectroscopic signature of Eu^{2+} and Eu^{3+}.[17] As the particles undergo a dry milling process [gray trace, Figure 2C], a decrease in the amount of Eu^{2+} is observed. As this data is taken with the total electron yield detection method, we expect some level of surface sensitivity to exist in our data. Therefore, the data suggests a surface layer (on the order of 10 nm) that is rich in Eu^{3+}. For quantification of the ratio between the oxidation states of Eu (Eu^{3+}/Eu^{2+}), multiplet simulations using the CTM4XAS program[18] were performed (bottom traces, Figure 2D). A "best fit" to the Eu M_5-edge data is achieved assuming a linear combination of the theoretical $Eu^{3+/2+}$ components. In our analysis, we assume the photoionization cross sections do not change between Eu^{2+} and Eu^{3+} which allows us to interpret the peak integrated area ratios as the valence ratios. Prior literature[19] suggests that XAS derived peak ratios agree quantitatively with Eu oxidation state ratios obtained via other analytical methods. As seen by eye, the Eu^{2+} component decreases with milling. This data indicates a Eu^{3+}/Eu^{2+} of ∼75%/25% and ∼85%/15% (±5%), for the as purchased and dry milled samples, respectively. We note, however, that any changes in the photoionization cross sections would affect the derived values equally, as the Eu^{3+} cross section could be a bit larger,[20] suggesting the Eu^{3+} component could be slightly overestimated in our analysis. It should be noted, however, that any small differences in photoionization cross section could not account for any changes in our conclusions, as the surface will still be populated primarily with Eu^{3+}.

As the SXANES experiments are sensitive to the surface, we used Eu L_3-edge HXANES measurements to investigate the bulk electronic structure of these materials. The Eu L_3-edge HXANES is plotted in Figure 3A and, like the soft X-ray experiments, suggests a mixed $Eu^{2+/3+}$ oxidation state. Unlike the SXANES, however, the HXANES, which are recorded in the partial fluorescence yield (PFY) mode, indicates a predominance of Eu^{2+} over the Eu^{3+} species. Using a data reduction method of an arctangent function to represent free election contribution to the line shape,[21] two Gaussian peaks were used to deconvolute the fraction of Eu^{2+} and Eu^{3+} present in the system (Figure 3A).

Using this method, we obtain a valence state population of ∼80% for Eu^{2+} and 20% for Eu^{3+} with this ratio not changing with milling (within experimental error). As the PFY technique is sensitive to the bulk, our combined XAFS measurements suggest that the particles are predominately Eu^{2+}, with a surface rich Eu^{3+} layer. The extended XAFS (EXAFS) region (Figure 3B) is extracted from Figure 3A using the ATHENA software package.[22] We note that, although the data is noisy, we can observe scattering contributions out to $k \sim 10$ Å^{-1} for the as purchased sample. Following milling, a reduction in EXAFS oscillations is

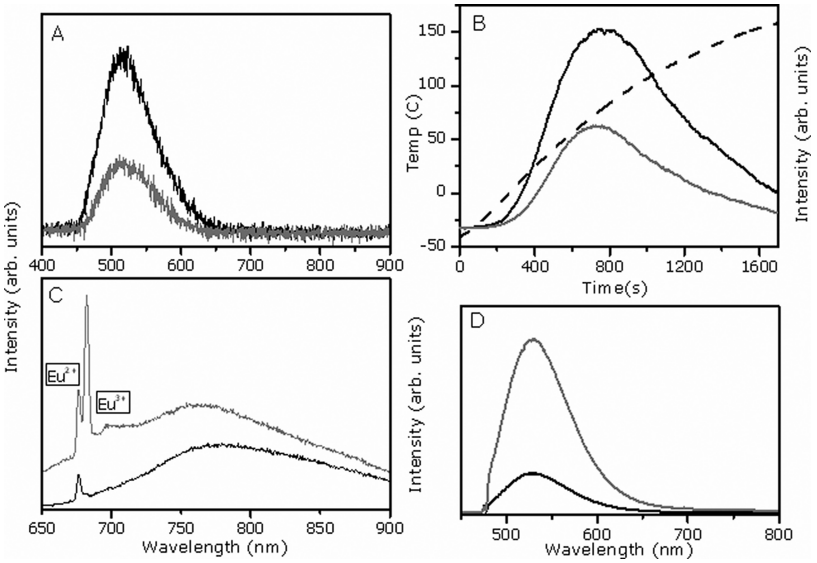

Figure 4. Comparison of (A) phosphorescence spectra and (B) integrated thermoluminescence versus sample temperature for the as purchased (black) and 48 h milled (gray) samples. Laser stimulated emission spectra, of the same samples, under continuous (C) 632 nm and (D) 473 nm excitation.

observed, likely to changes in the Deybe-Waller factors as the particle size is reduced.[23]

The Fourier transform (FT) of the EXAFS signal ($2 < k < 10$ Å^{-1}) is plotted in Figure 3C and represents a pseudoradial function that allows determination of the backscattering atoms (i.e., nearest neighbors). The first scattering contribution at ~2 Å is from O atoms, consistent with EXAFS results on Eu_2O_3.[24] The second scattering contribution at ~2.7 Å is due to scattering from Al atoms. This assignment is consistent with reported EXAFS derived *R* values for rare earth/aluminum alloys[25] and most likely excludes Eu−Eu scattering events as it has been shown that these contributions occur at $R > 3.5$ Å.[24,26] To fully understand the EXAFS results, we performed XAFS calculations using the ab initio code FEFF9.[27] For the calculations, a FEFF input file was created using the $SrAl_2O_4$ crystal structure with Sr as the absorbing atom. We then modified the FEFF input file with Eu as the absorbing atom, leaving all the other structural parameters the same. After the calculation, the theoretical spectrum was imported into the ATHENA program and followed the same data reduction parameters as performed on the experimental samples. The FT EXAFS of the theoretical spectrum is plotted in Figure 3C (bottom trace). The overlap between experimental spectrum for the as purchased sample and theory is very good, suggesting the local environment is not strongly affected by milling. Upon milling, we see a shift to lower *R* in the FT EXAFS for the first shell contributor of oxygen, a result consistent with the XRD data which suggests a milling induced reduction in lattice parameters (Figure 1B). Our combined XAFS and XRD results provide a good chemical and structural model for our system: Eu ions substitute for Sr sites in the monoclinic $SrAl_2O_4$ lattice, do not cluster, and exist in a dual oxidation state, with the Eu^{3+} located near the surface of the nanoparticle. Upon milling, we see a reduction in average nanoparticle size, an increase in Eu^{3+} species, and a reduction in lattice parameters.

For optical characterization, equivalent masses of the as purchased and 48 h milled samples were compared. Consistent with previously reported results, the phosphorescence spectra for both the milled and as purchased samples indicates broad green emission as shown in Figure 4A where the phosphorescence spectra collected after 1 min following optical excitation are compared. The decay indicates a persistent reduced phosphorescence emission for the milled samples (decay curve not shown). This decrease in the total emission of the milled samples can be attributed to an increased Eu^{3+}/Eu^{2+} ratio, caused by oxidation of Eu^{2+} during the milling process, as described by the XAFS results above. Interestingly, no apparent blue shift in the phosphorescence spectrum is observed for the ~150 nm milled particles, indicating a minimal effect on the oxidation state or the electronic energy levels of the codoped Dy^{3+} ions, which are thought to act as long-lived hole traps resulting in long afterglow in this system,[28] a result consistent with the SXANES analysis (Figure 2B). This is further evidenced by the conserved thermoluminescence behavior (Figure 4B), which exhibits a proportional decrease in signal, but no change in line shape. We note that, although Dy^{3+} is generally thought to act as an electronic trap, in certain conditions Dy^{3+} has been shown to act as a hole trap.[29] As our synthesized materials resemble those found in ref 29, we invoke a hole trapping mechanism, although we do note that our data does not exclusively point to such a mechanism.

While the phosphorescence and thermoluminescence data indicates an approximately 50% decrease in emission efficiency, the emission due to continuous laser stimulation at both 473 nm (continuous wave diode pumped solid laser) and 632 nm (continuous wave He−Ne), shown in Figure 4B,C, respectively, exhibits an increase in efficiency for the milled samples. While the specific mechanism for the strong short-lived visible emission (fluorescence) is still being investigated, it also appears to be commensurate with the relative abundance of Eu^{3+}, as indicated by the visible atomic absorption lines in the long wavelength spectrum (Figure 4C),[30] though accurate assignment of Eu peaks is tenuous in this matrix.

In conclusion, we present here a compositional and luminescence comparison of as purchased and mechanically milled $SrAl_2O_4$:Eu, Dy phosphor particles. While size reduction did result in improved solution stability, a nearly 50% decrease in phosphorescence and thermoluminescence yield resulted when nanoparticle dimensions were reduced to 150 nm. This indicates that sensible limits for size reduction by the milling technique

must be considered for this system to remain effective as a phosphor. Also, the presence of only Eu^{2+} and Eu^{3+} oxidation states suggest that the mechanism for phosphorescence of these materials is governed by $Eu^{2+/3+}$ redox complexes, versus participation of Eu^{+} species.[6] Interestingly, a sizable increase in stimulated emission was observed for the milled samples. This suggests that this material system may have further interest in solid state fluorescence applications.

AUTHOR INFORMATION

Corresponding Author

*E-mail: robert.meulenberg@maine.edu. Phone: 207-581-2245.

ACKNOWLEDGMENT

The authors acknowledge EDOTS Technology, LLC, and the Maine Technology Institute (DA2155) for financial support. The authors thank D. Brehmer, M. Lattimer, and E. Nelson of the SSRL for technical assistance at the beamline. Portions of this research were carried out at the SSRL, a national user facility operated by Stanford University on behalf of the U.S. Department of Energy, Office of Basic Energy Sciences.

REFERENCES

(1) Kim, J. S.; Sohn, K.-S.; Kwon, Y.-N.; Ban, G. S.; Lee, K. H. *Mater. Sci. Forum* **2007**, *539−542*, 2264–2268.
(2) Katsumata, T.; Mochida, S.; Kubo, H.; Usui, Y.; Aizawa, H.; Komuro, S.; Morikawa, T. *Proc. SPIE* **2005**, *5855*, 727–730.
(3) Yen, W. M., Shionoya, S., Yamamoto, H., Eds. *Practical Applications of Phosphors*; Boca Raton: CRC Press, 2006.
(4) Mishra, S. B.; Mishra, A. K.; Luyt, A. S.; Revaprasadu, N.; Hillie, K. T.; Steyn, W. J. V.; Coetsee, E.; Swart, H. C. *J. App. Polymer Sci.* **2010**, *115*, 579–587.
(5) de Chermont, Q. L.; Chaneac, C.; Sequin, J.; Pelle, F.; Maitrejean, S.; Jolivet, J. P.; Gourier, D.; Bessodes, M.; Scherman, D. *Proc. Natl. Acad. Sci. U.S.A.* **2007**, *104*, 9266–9271.
(6) Van den Eeckhout, K.; Smet, P. F.; Poelman, D. *Materials* **2010**, *3*, 2536–2566.
(7) Chander, H.; Haranath, D.; Shanker, V.; Sharma, P. *J. Cryst. Growth* **2004**, *271*, 307–312.
(8) Aruna, S. T.; Mukasyan, A. S. *Curr. Opin. Solid State Mater. Sci.* **2008**, *12*, 44–50.
(9) Wang, B.; Zhuo, Z.; Zhongyuan, L. U. *J. Wuhan Univ. Technol., Mater. Sci. Ed.* **2006**, *21*, 120–122.
(10) Katsumata, T.; Sakai, R.; Komuro, S.; Morikawa, T. *J. Electrochem. Soc.* **2003**, *150*, H111–H114.
(11) Nelson, A. J.; van Buuren, T.; Bostedt, C.; Schaffers, K. I.; Terminello, L. J.; Engelhard, M.; Baer, D. *J. Appl. Phys.* **2002**, *91*, 5135–5140.
(12) Levin, I.; Kaplan, W. D.; Brandon, D. G.; Müllejans, H.; Rühle, M. *Mater. Sci. Forum* **1996**, *207−209*, 749–752.
(13) Huang, W. L.; Labis, J.; Ray, S. C.; Liang, Y. R.; Pao, C. W.; Tsai, H. M.; Du, C. H.; Pong, W. F.; Chiou, J. W.; Tsai, M.-H.; Lin, H. J.; Lee, J. F.; Chou, Y. T.; Shen, J. L.; Chen, C. W.; Chi, G. C. *Appl. Phys. Lett.* **2010**, *96*, 062112.
(14) Yang, J. K.; Kim, W. S.; Park, H. H. *Thin Solid Films* **2006**, *494*, 311–314.
(15) Soldatov, A. V.; Povahzynaja, N. A.; Shvejtzer, I. G. *Solid State Commun.* **1996**, *97*, 53–58.
(16) Qi, Z. M.; Shi, C. S.; Liu, M.; Zhou, D. F.; Luo, X. X.; Zhang, J.; Xie, Y. N. *Phys. Status Solidi A* **2004**, *201*, 3109–3112.
(17) Krishnamurthy, V. V.; Lang, J. C.; Haskel, D.; Keavney, D. J.; Srajer, G.; Robertson, J. L.; Sales, B. C.; Mandrus, D. G.; Singh, D. J.; Bilc, D. I. *Phys. Rev. Lett.* **2007**, *98*, 126403.
(18) Stavitski, E.; de Groot, F. M. F. *Micron* **2010**, *41*, 687–694.
(19) Tanaka, T.; Yamamoto, T.; Kohno, Y.; Yoshida, T.; Yoshida, S. *Jpn. J. Appl. Phys.* **1999**, *38−1*, 30–35.
(20) Aylikci, V.; Apaydin, G.; Tiraşoğlu, E.; Kaya, N.; Cengiz, E. *Chem. Phys.* **2007**, *332*, 348–352.
(21) Krishnamurthy, V. V.; Keavney, D. J.; Haskel, D.; Lang, J. C.; Srajer, G.; Sales, B. C.; Mandrus, D. G.; Robertson, J. L. *Phys. Rev. B* **2009**, *79*, 014426.
(22) Ravel, B.; Newville, M. *J. Synchrotron Radiat.* **2005**, *12*, 537–541.
(23) Carta, D.; Casula, M. F.; Falqui, A.; Loche, D.; Mountjoy, G.; Sangregorio, C.; Corrias, A. *J. Phys. Chem. C* **2009**, *113*, 8606–8615.
(24) Ghosh, P.; Priolkar, K. R.; Patra, A. *J. Phys. Chem. C* **2007**, *111*, 571–578.
(25) Bacewicz, R.; Antonowicz, J. *Scr. Mater.* **2006**, *54*, 1186–1191.
(26) Tan, X.; Fan, Q.; Wang, X.; Grambow, B. *Environ. Sci. Technol.* **2009**, *43*, 3115–3121.
(27) Rehr, J. J.; Kas, J. J.; Vila, F. D.; Prange, M. P.; Jorissen, K. *Phys. Chem. Chem. Phys.* **2010**, *12*, 5503–5513.
(28) Luitel, H. N.; Watari, T.; Torikai, T.; Yada, M. *Res. Lett. Mater. Sci.* **2009**, *91*, 475074.
(29) Aizawa, H.; Katsumata, T.; Takahashi., J.; Matsunaga, K.; Komuro, S.; Morikawa, T.; Toba, E. *Electrochem. Solid-State Lett.* **2002**, *5*, H17–H19.
(30) Monteiro, M. A. F.; Brito, H. F.; Felinto, M.C.F.C.M.; Brito, G. E. S.; Teotonio, E. E. S.; Vichi, F. M.; Stefani, R. *Microporous Mesoporous Mater.* **2009**, *108*, 237–246.